

ARTICLE OPEN

Excitation to defect-bound band edge states in two-dimensional semiconductors and its effect on carrier transport

Dan Wang¹, Dong Han², Damien West³, Nian-Ke Chen¹, Sheng-Yi Xie¹, Wei Quan Tian⁴, Vincent Meunier³, Shengbai Zhang^{1,3} and Xian-Bin Li^{1,3}

The ionization of dopants is a crucial process for electronics, yet it can be unexpectedly difficult in two-dimensional materials due to reduced screening and dimensionality. Using first-principles calculations, here we propose a dopant ionization process for two-dimensional semiconductors where charge carriers are only excited to a set of defect-bound band edge states, rather than to the true band edge states, as is the case in three-dimensions. These defect-bound states have small enough ionization energies but large enough spatial delocalization. With a modest defect density, carriers can transport through band by such states.

npj Computational Materials (2019)5:8; <https://doi.org/10.1038/s41524-018-0145-0>

INTRODUCTION

Two-dimensional (2D) semiconductors beyond graphene, such as transition metal dichalcogenides,^{1–3} boron nitride,^{2,4,5} black phosphorus,^{6–8} group-III chalcogenides,^{9,10} and thin layers of topologically insulating Bi₂Te₃, Bi₂Se₃, and Sb₂Te₃¹¹ have attracted considerable attention in recent years. Their unique advantages in scaling semiconductors into atomic layers have raised the prospect of possible continuation of the Moore's Law.^{12,13} One such example is the recently proposed 2D MoS₂-based metal-oxide-semiconductor field-effect transistor which features a gate length of only 1 nm but excellent switching characteristics and an on-off current ratio of 10⁶.¹⁴ To broaden the applications in electronics, however, it is desirable to dope these 2D semiconductors by impurities,^{12,13,15} which is a standard procedure for carrier transport in three-dimensional (3D) semiconductors. For instance, to fabricate silicon-based complementary-metal-oxide-semiconductor integrated circuits, silicon requires both p- and n-type doping.

Developing electronics based on 2D semiconductors can be complicated. First, a significant reduction of the dielectric constant ϵ from 3D to 2D can be expected, which will adversely impact carrier ionization from dopants. Second, several theoretical studies have predicted that ionization energy in 2D semiconductors can be deeper than that in their 3D counterparts, well beyond the reduction of ϵ .^{16–19} As such, the difficulty in ionizing dopants can make it particularly challenging to yield a reasonable carrier concentration. In spite of these difficulties, experiments have consistently shown a certain degree of n- or p-type conductivity in 2D semiconductors.^{20–24} This apparent contradiction hints that defect physics in 2D semiconductors could be qualitative different from that in 3D.

In this paper, we identify a unique ionization process of impurities for carrier transport in 2D semiconductors. While our

systematic examination by first-principles calculations of defects and impurities in a prototypical 2D semiconductor MoS₂ indeed reveals very deep ionization energies IE_{∞} , due to the reduced dimensionality and reduced electronic screening, there is also a substantial Coulomb binding $E_{db}(n)$ between charge carriers and ionized defects, where n is a quantum number in qualitative analogy to the hydrogenic model.²⁵ Hence, besides the fully ionized $n = \infty$ state, carriers in the ground state of defects can also be excited to a set of defect-bound band edge (DBBE) states with an excitation energy $IE_n = IE_{\infty} - E_{db}(n)$. In particular, the $n = 1$ state is spatially localized when compared to the $n = \infty$ state but noticeably more delocalized when compared to the ground state of the defect. Note that the hydrogenic model here is only a rather crude approximation. In the case of Re_{Mo}, for instance, the $n = 1$ DBBE state is above the conduction band minimum (CBM), which pushes the CBM down to form a new band whose effective mass at K is only 30% larger than that in defect-free system. This non-intuitive result may help reconcile theory with experiment on doping MoS₂ and pave the way for eventual applications of all the 2D materials for electronics.

RESULTS AND DISCUSSION

Formation energies and density of states

To evaluate defect ionization, we calculate both IE_{∞} and the density of states (DOS) of charge neutral state ($q = 0$). Here, defects include native defects, i.e., vacancies: V_S , V_{Mo} , and V_{2S} , and antisites: Mo_S , S_{Mo} , and Mo_{2S} with the (-2) , (-1) , (0) , $(+1)$, and $(+2)$ charge states, and extrinsic impurities, i.e., Nb_{Mo} and Re_{Mo} with the (-1) , (0) , and $(+1)$ charge states, respectively. Among the native defects, V_S has the lowest neutral formation energy as shown in Fig. 1a, which is in line with the relative ease to observe such defects in MoS₂.^{26,27} Other native defects have higher

¹State Key Laboratory on Integrated Optoelectronics, College of Electronic Science and Engineering, Jilin University, 130012 Changchun, China; ²State Key Laboratory of Luminescence and Applications, Changchun Institute of Optics, Fine Mechanics and Physics, Chinese Academy of Sciences, 130033 Changchun, China; ³Department of Physics, Applied Physics, & Astronomy, Rensselaer Polytechnic Institute, Troy, NY 12180, USA and ⁴College of Chemistry and Chemical Engineering, Chongqing University, Huxi Campus, 401331 Chongqing, China

Correspondence: X.-B. Li (lixianbin@jlu.edu.cn)

These authors contribute equally: Dan Wang, Dong Han, Damien West

Received: 15 April 2018 Accepted: 20 December 2018

Published online: 15 January 2019

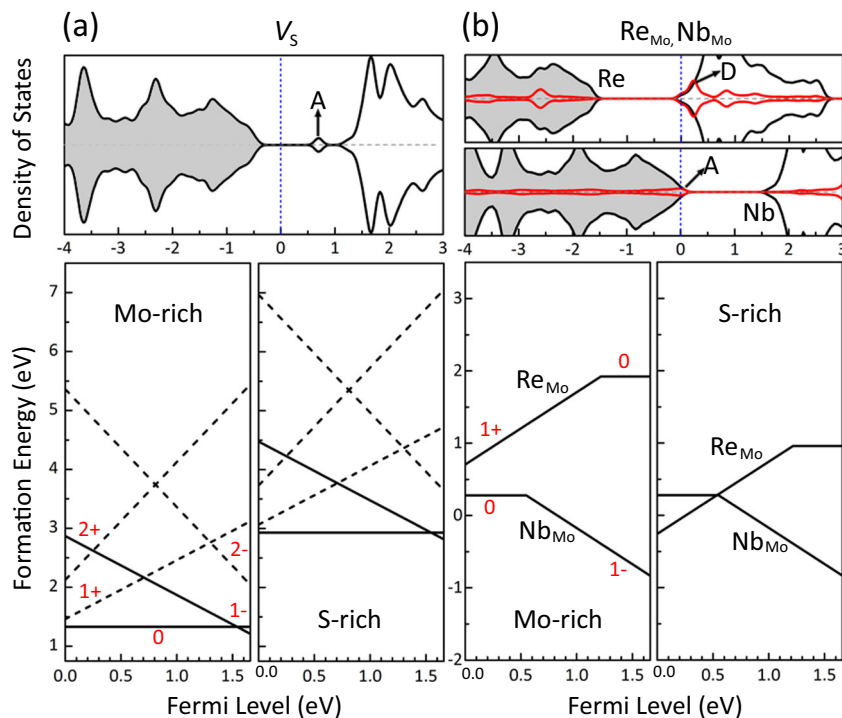


Fig. 1 Density states and formation energies of defects. Density of states and formation energies of **a** a typical intrinsic defect, V_S and **b** typical extrinsic dopants, Re_{Mo} and Nb_{Mo} in 2D MoS_2 . Acceptor and donor states are labeled with A and D in DOS, respectively. The local DOS for individual Re and Nb are also shown with a factor of 10 (red lines). Fermi level is set to 0 eV. The possible valences (noted by red number) of defects are fully considered for their formation energies under Mo- and S-rich condition

energies by at least a factor of 2, as can be seen in Figs. S1 and S2 in the Supplemental Materials (SM). According to Fig. 1b, extrinsic impurities Re_{Mo}/Nb_{Mo} have relatively low neutral formation energies too. Although both V_S and Re_{Mo}/Nb_{Mo} are low in energy, their electronic behaviors are qualitatively different. For example, V_S prefers to be in the charged states of (0) and (−1) with a transition level at $\epsilon(0/-1) = E_{VBM} + 1.55$ eV, where VBM denotes the valence band maximum (while CBM stands for the conduction band minimum). Hence, as an acceptor, its IE_∞ for holes is very large. The same deepness is quantitatively reflected by the deep gap states in the DOS. In contrast, IE_∞ 's for Re_{Mo} (donor) and Nb_{Mo} (acceptor) are 0.45 and 0.55 eV, respectively, which are high enough to prevent a full carrier ionization at room temperature. Here, we also used the revised Tao–Perdew–Staroverov–Scuseria meta-generalized gradient approximation (RTPSS meta-generalized gradient approximation (GGA)),²⁸ which is above the GGA rung in the “Jacob’s ladder” of approximations, to calculate IE_∞ for Re_{Mo} . The RTPSS results are similar to those of Perdew–Burke–Ernzerhof (PBE), e.g., with a vacuum region of 20 Å, the IE_∞ is 0.41 eV (PBE) and 0.39 eV (RTPSS), respectively. Note that RTPSS still underestimates the bandgap compared with many-body perturbation theory GW calculations and experiment.^{29,30} This suggests that the actual ionization energy may be even larger than what has been predicted here. However, according to the DOS computed for a finite cell size, both appear as delocalized states and are shallow with respect to the respective band edges, which suggests that there could be a delocalized-to-localized (or shallow-to-deep) transition for Re_{Mo} and Nb_{Mo} with the concentration of dopants.

Transition levels and Coulomb binding energies

As mentioned earlier, the binding energy of DBBE states can be rather significant. Figure 2 shows E_{db} ($n=1$), as well as the ground-state energy or transition level, with respect to the band edges (CBM and VBM) for donors and acceptors, respectively. We

see that, in 2D MoS_2 , $E_{db} = 0.25$ – 0.56 eV can be quite large. The details can be also found in Table S1 (Supplemental Materials). Therefore, in 2D semiconductors most charge carriers are bound carriers, oppose to be almost free in 3D semiconductors.

To understand why E_{db} can be so large, we again resort to the hydrogenic model. In a 3D system, the dielectric screening ϵ is usually large so the binding is weak as shown in Fig. 3.^{25,31,32} This leads to $E_{db}(n, 3D) = \frac{1}{n^2\epsilon^2} R_y$, where R_y is the Rydberg energy and n runs from 1 to ∞ . In analogy, for our 2D systems, the model yields $E_{db}(n, 2D) = \frac{1}{(n-1/2)^2\epsilon^2} R_y$. Numerical results are schematically shown in Fig. 3a for 3D and in Fig. 3b for 2D. Note that holes are mirror images of electrons with different effective masses. They are schematically illustrated in Fig. 3c for 3D and in Fig. 3d for 2D. The ratio of the binding energy between 2D and 3D = $E_{db}(n=1, 2D)/E_{db}(n=1, 3D)$ can be very important, which is enhanced by a factor of $4[\epsilon(3D)/\epsilon(2D)]^2$ for both electrons and holes. Here, we stress that the hydrogenic model is just used to qualitatively illustrate the fundamental difference between 2D and 3D in terms of Coulomb binding. The model has, however, not been used in any quantitative evaluation of the physical properties.

Spatial distribution of DBBE states

As mentioned earlier, the spatial distribution of $n=1$ DBBE state can be considerably different from that of defect ground state. Taking acceptors as an example, Fig. 4 shows the spatial distribution of the $n=1$ hole state for a number of native defects and Nb_{Mo} . Note that to study the spatial distribution, the supercell needs to be large enough. For this reason, we show in Fig. 4 two sets of results calculated with a small 147-atom supercell and a larger 507-atom cell. The 147-atom cell has been used to calculate E_{db} . The same trend in the localization of the DBBE states can be clearly seen in these two sets of calculations, and the holes become more and more localized with increasing E_{db} from 0.0 (no defect) to 0.44 eV.

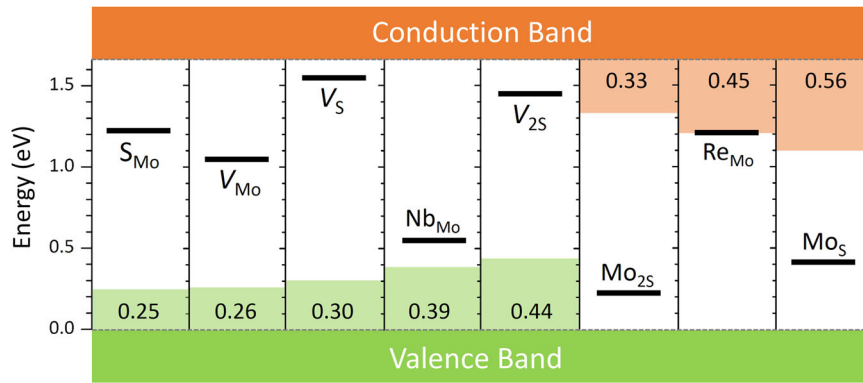


Fig. 2 Transition levels and binding energies. Binding energy between ionized carrier (at DBBE state) and its oppositely charged defect E_{db} ($n = 1$) in monolayer MoS_2 . The transition levels according to the IE_∞ (solid line) of acceptors ($0/-1$) and donors ($+1/0$) within the calculated band gap. The E_{db} are marked with color coding next to band edge: green for acceptors and orange for donors

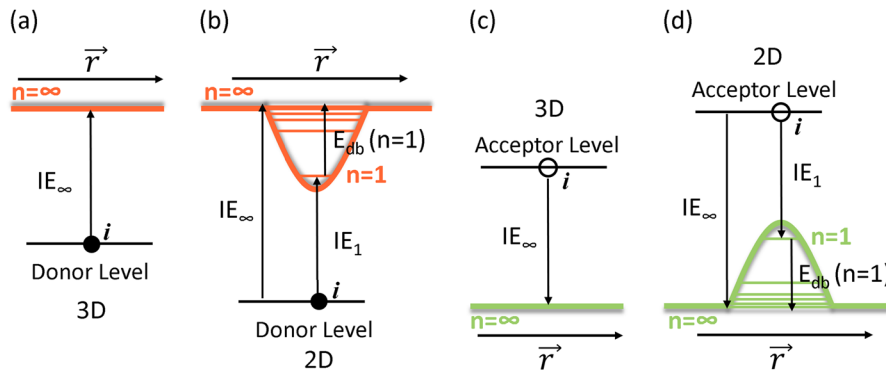


Fig. 3 Schematic illustration of charge-carrier ionizations in **a, c** 3D and **b, d** 2D semiconductors. Emphases have been placed on the 2D cases where IE_∞ is the energy of an electron or a hole completely removed from their respective defect states (labeled as i). Due to the Coulomb attraction by the ionized defect, there should be a set of bound states (derived from the band edge states), namely, the DBBE states discussed in the main text. IE_1 corresponds to moving a hole or an electron from the defect state i to $n = 1$ DBBE state, i.e., $IE_1 = IE_\infty - E_{db}(n = 1)$. Here, we have used the hydrogenic model for illustration purpose with the understanding that the model needs not represent a real defect. As such, the principal quantum number n here only indicates the order of the energy levels

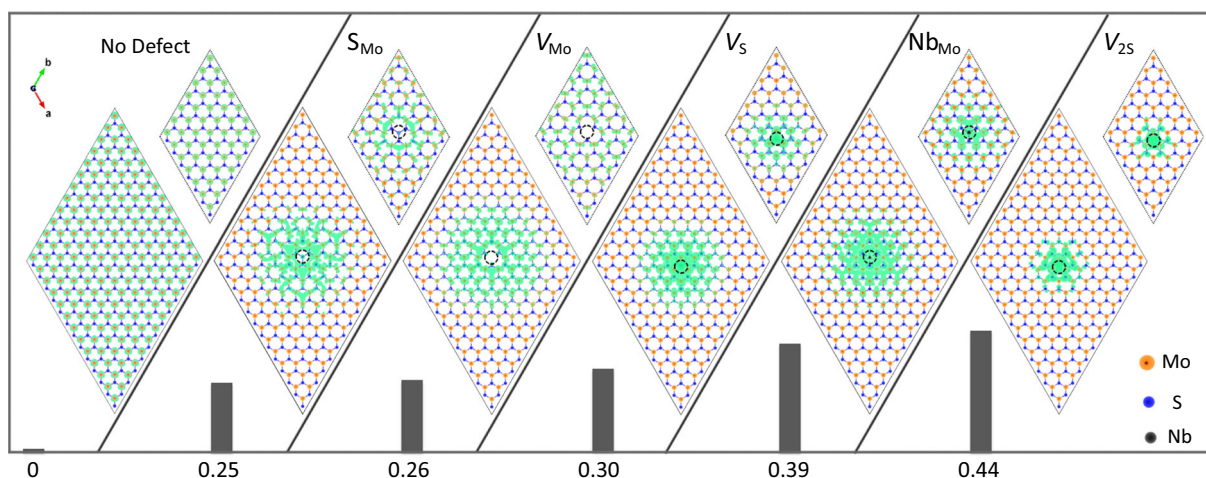


Fig. 4 Real-space distributions of $n = 1$ hole states for various acceptor-like defects in 2D MoS_2 , calculated by using a small 147-atom cell and a larger 507-atom cell. Green isosurface of density is set to 4×10^{-4} and $1.2 \times 10^{-4} e/a_0^{-3}$ for the small and larger cells, respectively, where a_0 is the Bohr radius. Circles at the center of the supercells denote the positions of the defects. Histograms at the bottom of the figure show the corresponding binding energies (E_{db})

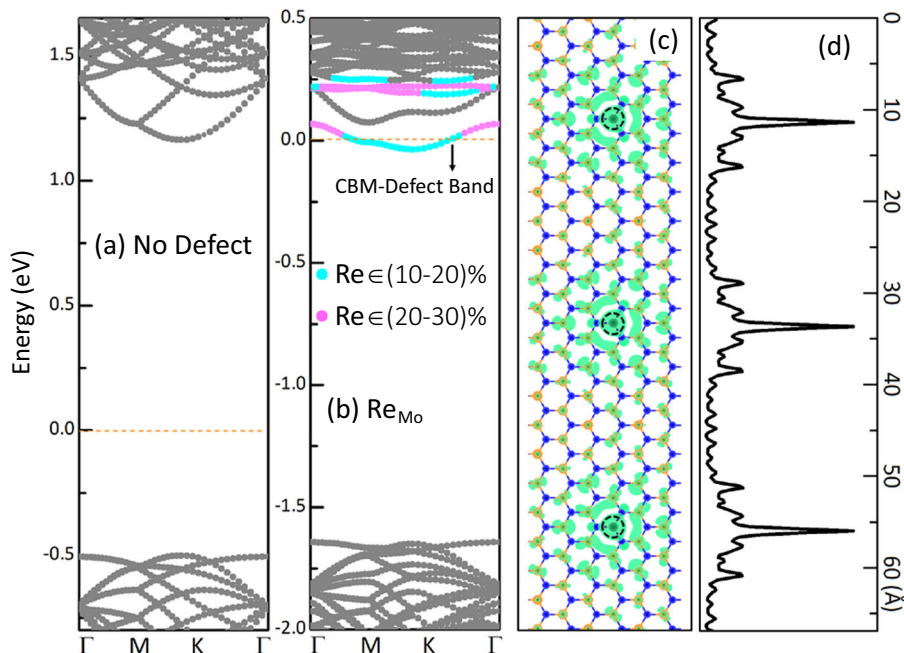


Fig. 5 Defect bound band edge transport with increasing defect density. Band structure of **a** no-defect and **b** Re-doped monolayer MoS₂ with a defect density of about 10^{13} cm^{-2} . The spatial distribution of the defect bound band **c** and its corresponding linear charge density **d**. The isosurface in **c** is $3 \times 10^{-4} e/a_0^{-3}$, where a_0 is the Bohr radius. Dashed circles denote the positions of the defects

The presence of a large E_{db} associated with the DBBE states resolves both of the aforementioned perplexing issues. Firstly, it explains the deep levels associated with Re_{Mo} and Nb_{Mo} that were found in the calculation of the ionization energy IE_{∞} . This can be traced back to the poor screening in the case of 2D semiconductors. As the ionization energy is the difference between the charged and neutral formation energies, $\varepsilon(q/0) = \frac{\Delta H(D^q) - \Delta H(D^0)}{q}$, the lack of screening means that the charged defect is closer to a bare charge, substantially increasing $\Delta H(D_q)$ relative to the 3D counterpart. Increasing the formation energy of the charged defects relative to the neutral defect naturally leads to an increase in the ionization energies. This, in turn, is linked with the large DBBE binding as the reduced screening opens the door for the ionized carriers to effectively screen the charged defects, substantially lowering the energy of the ionized carriers when in the DBBE states.

Carrier transport mechanism

Secondly, the large E_{db} points toward an experimental mechanism for conduction despite the large ionization energies associated with these defects. Re_{Mo} constitutes such an example with a relative small $\text{IE}_{\infty} = 0.45 \text{ eV}$. Yet, this IE_{∞} is large enough to prevent significant carrier excitation at room temperature. Most surprisingly, however, the lack of IE_1 in Re_{Mo} can be seen in Fig. 5 where the donor is spontaneously ionized. As a result, the pink Re_{Mo} -derived states in Fig. 5b are in fact above the CBM. It pushes down the bulk conduction band states. We propose that with a reasonable defect density, such as 10^{13} cm^{-2} in Qiu's study,³⁵ the pushed-down states form a band ideally suited for carrier conduction. To elaborate, Fig. 5c, d show the push-down states where a certain degree of charge overlap has been witnessed. Due to the presence of push-down states, electrons could transport through the band with an effective mass that is only 30% larger than that of the free electron at the CBM, as shown in Table S2 (Supplemental Materials).

In summary, our first-principles calculations identify a set of DBBE states, which could have pronounced effects on the defect ionization in 2D semiconductors. The reason for the formation of the DBBE states is the strong binding between charged ions and ionized charge carriers, leading to an extra channel for low-energy excitation. The strong binding is a result of the spatial confinement as well as the reduced screening in 2D materials. The experimentally observed conductivity in Re-doped MoS₂, on the other hand, could be a special case of DBBE-state transport where the $n = 1$ DBBE state enters the conduction band to push down the CBM. The present investigations suggest a unique picture of carrier ionization from defects and its implication to carrier transport in 2D semiconductors towards emerging nanoelectronic devices.

METHODS

Calculation of ionization energies IE_{∞}

All the calculations are performed within the density-functional theory (DFT)^{36,37} as implemented in the Vienna ab-initio simulation package (VASP).^{38,39} The projector-augmented plane wave basis and GGA with the PBE functional form are employed.⁴⁰ The cutoff energy for the plane wave basis is 520 eV and a $3 \times 3 \times 1$ Monkhorst-Pack mesh grid is used for k-point sampling. Spin polarization is included. The calculated lattice parameter is 3.185 Å and the PBE bandgap is 1.66 eV for 2D MoS₂, which agree well with previous calculation.¹⁷ To obtain the ionization energy (IE_{∞}) and the corresponding formation energy of the charge defect in 2D system, we use the extrapolation method in our previous work,¹⁸

$$\text{IE}_{\infty}(S, L_z) = \text{IE}_{\infty} + \frac{a}{\sqrt{S}} + \frac{\beta L_z}{S} \quad (1)$$

where $\text{IE}_{\infty}(S, L_z)$ is the size-dependent ionization energy, IE_{∞} is the true, size-independent ionization energy. S and L_z are lateral size and vacuum size, respectively. a is the defect-specific Madelung constant and $\beta = \frac{e^2}{24\epsilon_0}$. Note that this expression neglects higher order terms, which may not be negligible for thicker slabs.^{16,41,42} However, the error here for monolayer MoS₂ (0.31 nm thickness) should be substantially less than 0.1 eV according to our previous studies, for example, the error for monolayer black phosphorus (0.21 nm thickness) is 0.04 eV and the error for thicker bilayer

black phosphorus (0.77 nm thickness) is 0.13 eV.¹⁹ Here IE_{∞} is obtained at a fixed $L_z = 40 \text{ \AA}$ with $L_x \times L_y$ ranging from 5×5 to 7×7 . We have also tested the convergence of L_z for example, for V_S where $IE_{\infty} = 1.52, 1.52,$ and 1.55 eV , respectively, for $L_z = 20, 30,$ and 40 \AA .

Calculation of Coulomb binding energies E_{db}

The Coulomb binding of the charge carrier with the corresponding charged defect is calculated by a fixed occupation method⁴³ where we perform a constrained DFT calculation to treat the excited states. In the case when the defect state is degenerate, for example, the Sulphur vacancy acceptor (V_S), we consider different electronic configurations for the excited states: e.g., exciting one spin-up electron, one spin-down electron, or half spin-up and half spin-down electrons. The results show that the binding energies are unchanged to within a couple of tens meV.

DATA AVAILABILITY

The data that support the findings of this study are available from the corresponding author, Professor Xian-Bin Li (email: lixianbin@jlu.edu.cn) upon reasonable request.

ACKNOWLEDGEMENTS

Work in China was supported by National Natural Science Foundation of China (No. 11874171, No.11504368, No. 61775077, and No. 11704111). D.W. and S.Z. were supported by the Department of Energy under Grant No. DE-SC0002623. W.Q.T. thanks support from the Open Project of Key Laboratory of Polyoxometalate Science of Ministry of Education (NENU) and State Key laboratory of Supramolecular Structure and Materials (JLU) (No. SKLSSM201818). Also, we acknowledge the High-Performance Computing Center (HPCC) at Jilin University for calculation resources.

AUTHOR CONTRIBUTIONS

D. Wang, D.H., and D. West did the calculations. D. Wang, D. West, X.L., and S.B.Z. did the theoretical analyses. The paper is written by D. Wang, X. L., and S.B.Z. with the help from all the authors. D. West and S.B.Z. were actively engaged in the design and development of the theory, participated in all discussions, and draft of the manuscript. All the authors contributed to the interpretation of the results. X. L. proposed and initiated the project. D. Wang, D.H., and D. West contribute equally to this work.

ADDITIONAL INFORMATION

Supplementary information accompanies the paper on the *npj Computational Materials* website (<https://doi.org/10.1038/s41524-018-0145-0>).

Competing interests: The authors declare no competing interests.

Publisher's note: Springer Nature remains neutral with regard to jurisdictional claims in published maps and institutional affiliations.

REFERENCES

- Wang, Q. H., Kalantar-Zadeh, K., Kis, A., Coleman, J. N. & Strano, M. S. Electronics and optoelectronics of two-dimensional transition metal dichalcogenides. *Nat. Nanotech.* **7**, 699–712 (2012).
- Xu, M., Liang, T., Shi, M. & Chen, H. Graphene-like two-dimensional materials. *Chem. Rev.* **113**, 3766–3798 (2013).
- Xiao, J. et al. Nonlinear optical selection rule based on valley-exciton locking in monolayer ws_2 . *Light Sci. Appl.* **4**, e366 (2015).
- Pacilé, D., Meyer, J. C., Girit, Ç. Ö. & Zettl, A. The two-dimensional phase of boron nitride: few-atomic-layer sheets and suspended membranes. *Appl. Phys. Lett.* **92**, 133107 (2008).
- Slotman, G. J. & Fasolino, A. Structure, stability and defects of single layer hexagonal BN in comparison to graphene. *J. Phys. Condens. Matter* **25**, 045009 (2013).
- Li, L. et al. Black phosphorus field-effect transistors. *Nat. Nanotech.* **9**, 372–377 (2014).
- Qiao, J., Kong, X., Hu, Z. X., Yang, F. & Ji, W. High-mobility transport anisotropy and linear dichroism in few-layer black phosphorus. *Nat. Commun.* **5**, 4475 (2014).
- Yang, J. et al. Optical tuning of exciton and trion emissions in monolayer phosphorene. *Light Sci. Appl.* **4**, e312 (2015).
- Hu, P. et al. Highly responsive ultrathin GaS nanosheet photodetectors on rigid and flexible substrates. *Nano. Lett.* **13**, 1649–1654 (2013).

- Wang, D., Li, X. B. & Sun, H. B. Native defects and substitutional impurities in two-dimensional monolayer InSe. *Nanoscale* **9**, 11619–11624 (2017).
- Zhang, Y. et al. Crossover of the three-dimensional topological insulator Bi_2Se_3 to the two-dimensional limit. *Nat. Phys.* **6**, 584–588 (2010).
- Chhowalla, M., Jena, D. & Zhang, H. Two-dimensional semiconductors for transistors. *Nat. Rev. Mater.* **1**, 16052 (2016).
- Wang, D., Li, X.-B., Han, D., Tian, W. Q. & Sun, H.-B. Engineering two-dimensional electronics by semiconductor defects. *Nano Today* **16**, 30–45 (2017).
- Desai, Sujay B. et al. MoS_2 transistors with 1-nanometer gate lengths. *Science* **354**, 99–102 (2016).
- Zhang, S. B. The microscopic origin of the doping limits in semiconductors and wide-gap materials and recent developments in overcoming these limits: a review. *J. Phys. Condens. Matter* **14**, R881–R903 (2002).
- Noh, J.-Y., Kim, H. & Kim, Y.-S. Stability and electronic structures of native defects in single-layer MoS_2 . *Phys. Rev. B* **89**, 205417 (2014).
- Komsa, H.-P. & Krasheninnikov, A. V. Native defects in bulk and monolayer MoS_2 from first principles. *Phys. Rev. B* **91**, 125304 (2015).
- Wang, D. et al. Determination of formation and ionization energies of charged defects in two-dimensional materials. *Phys. Rev. Lett.* **114**, 196801 (2015).
- Wang, D. et al. Charged defects in two-dimensional semiconductors of arbitrary thickness and geometry: formulation and application to few-layer black phosphorus. *Phys. Rev. B* **96**, 155424 (2017).
- Radisavljevic, B., Radenovic, A., Brivio, J., Giacometti, V. & Kis, A. Single-layer MoS_2 transistors. *Nat. Nanotech.* **6**, 147–150 (2011).
- Li, H. et al. Optical identification of single- and few-layer MoS_2 sheets. *Small* **8**, 682–686 (2012).
- Li, H. et al. Fabrication of single- and multilayer MoS_2 film-based field-effect transistors for sensing NO at room temperature. *Small* **8**, 63–67 (2012).
- Laskar, M. R. et al. p-type doping of MoS_2 thin films using Nb. *Appl. Phys. Lett.* **104**, 092104 (2014).
- Suh, J. et al. Doping against the native propensity of MoS_2 : degenerate hole doping by cation substitution. *Nano. Lett.* **14**, 6976–6982 (2014).
- Chuang, S. L. *Physics of Optoelectronic Devices* (Wiley, New York, 1995).
- Zhou, W. et al. Intrinsic structural defects in monolayer molybdenum disulfide. *Nano Lett.* **13**, 2615–2622 (2013).
- Hong, J. et al. Exploring atomic defects in molybdenum disulphide monolayers. *Nat. Commun.* **6**, 6293 (2015).
- Perdew, J. P., Ruzsinszky, A., Csonka, G. I., Constantin, L. A. & Sun, J. Workhorse semilocal density functional for condensed matter physics and quantum chemistry. *Phys. Rev. Lett.* **103**, 026403 (2009).
- Rasmussen, F. A. & Thygesen, K. S. Computational 2D materials database: electronic structure of transition-metal dichalcogenides and oxides. *J. Phys. Chem. C* **119**, 13169–13183 (2015).
- Qiu, D. Y., da Jornada, F. H. & Louie, S. G. Screening and many-body effects in two-dimensional crystals: monolayer MoS_2 . *Phys. Rev. B* **93**, 235435 (2016).
- Klingshirn, C. F. *Semiconductor Optics*. 2nd ed (Springer, Berlin, 2007).
- Wannier, G. H. The structure of electronic excitation levels in insulating crystals. *Phys. Rev.* **52**, 191–197 (1937).
- Chernikov, A. et al. Exciton binding energy and nonhydrogenic Rydberg series in monolayer WS_2 . *Phys. Rev. Lett.* **113**, 076802 (2014).
- Olsen, T., Latini, S., Rasmussen, F. & Thygesen, K. S. Simple screened hydrogen model of excitons in two-dimensional materials. *Phys. Rev. Lett.* **116**, 056401 (2016).
- Qiu, H. et al. Hopping transport through defect-induced localized states in molybdenum disulphide. *Nat. Commun.* **4**, 2642 (2013).
- Hohenberg, P. & Kohn, W. Inhomogeneous electron gas. *Phys. Rev.* **136**, B864–B871 (1964).
- Kohn, W. & Sham, L. J. Self-consistent equations including exchange and correlation effects. *Phys. Rev.* **140**, A1133–A1138 (1965).
- Kresse, G. & Furthmüller, J. Efficient iterative schemes for ab initio total-energy calculations using a plane-wave basis set. *Phys. Rev. B* **54**, 11169–11186 (1996).
- Kresse, G. & Furthmüller, J. Efficiency of ab-initio total energy calculations for metals and semiconductors using a plane-wave basis set. *Comput. Mater. Sci.* **6**, 15–50 (1996).
- Perdew, J.P., Burke, K. & Ernzerhof, M. Generalized gradient approximation made simple. *Phys. Rev. Lett.* **77**, 3865–3868 (1996).
- Wu, F., Galatas, A., Sundararaman, R., Rocca, D. & Ping, Y. First-principles engineering of charged defects for two-dimensional quantum technologies. *Phys. Rev. Mater.* **1**, 071001(R) (2017).
- Naik, M. H. & Jain, M. CoFFEE: corrections for formation energy and eigenvalues for charged defect simulations. *Comput. Phys. Commun.* **226**, 114–126 (2018).
- Kaduk, B., Kowalczyk, T. & Van Voorhis, T. Constrained density functional theory. *Chem. Rev.* **112**, 321–370 (2011).



Open Access This article is licensed under a Creative Commons Attribution 4.0 International License, which permits use, sharing, adaptation, distribution and reproduction in any medium or format, as long as you give appropriate credit to the original author(s) and the source, provide a link to the Creative Commons license, and indicate if changes were made. The images or other third party material in this article are included in the article's Creative Commons license, unless indicated otherwise in a credit line to the material. If material is not included in the

article's Creative Commons license and your intended use is not permitted by statutory regulation or exceeds the permitted use, you will need to obtain permission directly from the copyright holder. To view a copy of this license, visit <http://creativecommons.org/licenses/by/4.0/>.

© The Author(s) 2019